## Manipulability Maximization of a Liquid-Handling Manipulator for Sloshing Suppression via Container Tilting

Ryuji Nakagawa<sup>©</sup> and Ryosuke Tasaki<sup>©</sup>
Department of Mechanical Engineering, Aoyama Gakuin University, Sagamihara, Kanagawa, Japan

Keywords: Manipulability, Sloshing Suppression, Optimization Problem, Trajectory Constraint.

Abstract:

The manipulability index measures a robot's motion capability. To avoid singularity problems and to achieve unexpected changes in tasks, a method that explicitly considers this metric is needed. However, the index is a nonlinear function that depends on the state of the manipulator, making optimization difficult in a short period of time. In addition, real-time control of the robot, which requires computational efficiency, is necessary to ensure safety in a dynamic environment. Previous studies have generated trajectories that increase this metric, but different tasks require different constraints to be considered. Controlling not only the trajectory but also the posture and velocity of the end-effector expands the area of practical use. In this paper, we formulate a manipulability optimization problem for real-time control in liquid transfer and solve it efficiently using inequality constraints. In liquid transfer experiments, the method successfully generates safe and kinematic trajectories with high performance by optimizing both manipulability and controlling velocity and attitude to suppress liquid surface vibration.

#### 1 INTRODUCTION

Recent advances in collaborative robots have responded to the shift from high-volume to high-mix production, with increasing demand driven by their flexibility in adapting to complex tasks (Kavraki et al., 1996). Unlike industrial robots, collaborative robots operate safely alongside humans without traditional safety barriers. In Human-Robot Collaboration (HRC) spaces, safety remains a primary concern. Various motion planning approaches, including RRT and CHOMP, address collision avoidance and task constraints (LaValle & Kuffner, 2001; Wang et al., 2019). However, dynamic environments demand that robots rapidly adapt to unpredictable situations, requiring trajectories that maintain high kinematic performance. The manipulator's posture critically affects adaptability (Haowen et al., 2024); poor configurations limit responsive movements.

The manipulability ellipsoid (Yoshikawa, 1985) describes the robot's directional motion capability, and the manipulability index—proportional to ellipsoid volume—assesses proximity to singularities.

Maximizing this index enhances adaptability in dynamic environments. Dufour et al. integrated a linearized manipulability index into inverse kinematics using Quadratic Programming (2020). Other methods, such as Gaussian process regression for trajectory optimization (Maric et al., 2019) and neural networks (Jin et al., 2017), have also been proposed. More recently, manipulability optimization has been applied to multi-arm coordination (Kennel-Maushart et al., 2021) and human–robot collaboration tasks (Zhang, 2022). However, most studies address manipulability improvement or task-specific constraints separately, and few have integrated them into a unified framework.

In parallel, liquid transfer with open containers is another challenging problem, where sloshing suppression has been studied through trajectory shaping and container tilting strategies (Yano & Terashima, 2001; Moriello et al., 2018; Muchacho et al., 2022). These methods effectively reduce liquid oscillations but generally ignore the kinematic performance of the manipulator, limiting their applicability in tasks that require both stability and adaptability.

alp https://orcid.org/0009-0001-0525-5729 blp https://orcid.org/0000-0002-3619-4498

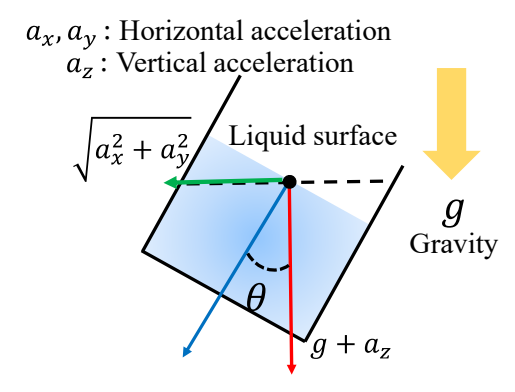


Figure 1: Schematic of sloshing suppression control.

This study proposes a trajectory optimization framework that maximizes the manipulability index while simultaneously suppressing liquid vibrations. A key feature of the formulation is that sloshing suppression is expressed as an inequality constraint rather than as part of the objective function. This keeps the objective lightweight and computationally efficient, while the introduction of flexible constraints allows the feasible range to be adaptively adjusted, reducing computational load without sacrificing task feasibility. These characteristics make the approach suitable for real-time implementation in dynamic environments. Effectiveness is validated through experiments with a 7-DOF manipulator performing liquid transfer tasks, confirming that the proposed method achieves safe and kinematically efficient trajectories that enhance manipulability while suppressing sloshing.

### 2 PRINCIPLE OF SLOSHING SUPPRESSION

Sloshing suppression during liquid transfer has been extensively studied, with approaches including CFD-based modeling (Muller et al., 2003; Diavareshkian & Khalili, 2006) and filtered trajectory generation targeting vibration frequencies (Yano et al., 2001; Yano & Terashima, 2001). These typically assume horizontal container orientation in linear systems. In contrast, manipulator-based studies explore container tilting to counteract acceleration-induced liquid motion (Moriello et al., 2018; Muchacho et al., 2022).

This study proposes a trajectory optimization method that dynamically adjusts container orientation based on acceleration while enhancing the manipulability index. The vibration control strategy is detailed in this chapter.

### 2.1 Statement of Tilting Method

Figure 1 illustrates the schematic of the proposed sloshing suppression control method. Vibration is mitigated by minimizing horizontal acceleration within the container, achieved by aligning the container's orientation with the direction of the applied acceleration. The container's tilt angle  $\theta$  [rad] is calculated based on the horizontal accelerations  $\alpha_x$  and  $\alpha_y$  [m/s²], the vertical acceleration  $\alpha_z$  [m/s²], and gravitational acceleration g [m/s²].

$$\theta = \tan^{-1} \frac{\sqrt{\alpha_x^2 + \alpha_y^2}}{(g + \alpha_z)} \tag{1}$$

In essence, sloshing is suppressed when the net acceleration vector acting on the liquid aligns with the normal vector of the liquid surface.

### 2.2 Acceleration Smoothing

As shown in (1), the manipulator adjusts the container's tilt in response to acceleration. However, abrupt changes in acceleration, such as step inputs, can result in infeasible motion due to excessive speed requirements. To ensure feasibility, the acceleration profile must be smooth. By regulating the rate of change of acceleration, the manipulator generates motion within its operational limits.

The rate of change of acceleration is referred to as jerk. A low-jerk trajectory ensures smooth acceleration, enabling the desired tilt of the container. Accordingly, the optimal trajectory is obtained by minimizing jerk, as defined by the evaluation function below, where x(t) denotes position.

$$J(x(t)) = \int_0^T \left(\frac{d^3x(t)}{dt^3}\right)^2 dt \tag{2}$$

The functional reaches its extremum when x(t) satisfies the Euler-Poisson equation, allowing the trajectory to be expressed as a fifth-order polynomial.

$$x(T) = x_0 + (x_f - x_0)(6T^5 - 15T^4 + 10T^3)$$

$$-v_0(3T^5 - 8T^4 + 6T^3 - T)$$

$$-v_f(3T^5 - 7T^4 + 4T^3)$$

$$-0.5a_0(T^5 - 3T^4 + 3T^3 - T^2)$$

$$+0.5a_f(T^5 - 2T^4 + T^3)$$

$$T = \frac{t}{t_f}$$
(4)

where x, v, and a represent the position, velocity, and acceleration, respectively, while the subscripts 0 and f denote the starting and ending points. Equation (4) is scaled by the final time  $t_f$ . This is known as the minimum jerk model (Flash & Hogan, 1985), which generates a trajectory with minimal jerk based on the current state and the endpoint state. In this study, the trajectory generated using this model is referred to as the minimum jerk trajectory. When the container is transported along a smooth acceleration, the lateral acceleration of the liquid is cancelled by tilting the container.

### 3 MANIPULATOR KINEMATICS AND MANIPULABILITY

Manipulator kinematics consists of forward kinematics, which computes the end-effector pose from joint angles, and inverse kinematics, which determines joint configurations for a desired task-space pose. The manipulability index, derived from the Jacobian, reflects the manipulator's motion capability.

### 3.1 Kinematics and Manipulability

The forward kinematics of a manipulator with n degrees of freedom at joint configuration  $q \in \mathbb{R}^n$  is expressed as

$$x = f(q) \tag{5}$$

where  $x \in \mathbb{R}^m$  is the end-effector pose (position and orientation in task space) and  $f(\cdot)$  is a nonlinear mapping. Since solving this relation directly is often computationally demanding, it is commonly linearized through differential kinematics:

$$\dot{x} = I(q)\dot{q} \tag{6}$$

where  $\dot{x} = [v^T \omega^T]^T \in \mathbb{R}^m$  represents the linear velocity v and angular velocity  $\omega$  of the end-effector, and  $\dot{q}$  is the joint velocity vector. The Jacobian matrix  $J(q) \in \mathbb{R}^{m \times n}$  maps joint velocities to task-space velocities. In this context, J(q) represents the manipulator Jacobian, distinct from the cost functional J(x(t)) defined in (2).

Manipulability is an important index in motion planning, and increasing it allows for greater flexibility in motion and avoidance of singularities. This index is defined as follows

$$m(q) = \sqrt{\det(J(q)J(q)^T)} = \prod_{i=1}^n \sigma_i$$
 (7)

where  $\sigma_i$  are the singular values of J(q). Since  $\sigma_i > 0$ , m(q) > 0. If m(q) is close to 0, the manipulator is close to a singular configuration. Conversely, larger values correspond to configurations that allow greater dexterity and adaptability.

### 3.2 Manipulability Optimization

Optimization-based motion planning enables robots to generate efficient and safe trajectories under task-specific constraints. In manipulability optimization, the objective is to maximize m(q), thereby enhancing motion flexibility and avoiding singularities. The problem is formulated as:

$$\min_{q} m(q) \tag{8}$$

Subject to

$$\dot{x} = J(q)\dot{q}$$

$$q^{-} \le q \le q^{+}$$

$$\dot{q}^{-} \le \dot{q} \le \dot{q}^{+}$$

where  $q^+$  and  $q^-$  are the upper and lower limits of the joint angle, and  $\dot{q}^+$  and  $\dot{q}^-$  are the joint velocity limits. Maximizing m(q) is crucial for generating trajectories that exhibit high motion performance, enhancing the overall agility and efficiency of the manipulator.

The gradient of the manipulability index is required for iterative optimization. In this study, the gradient is computed numerically using finite differences:

$$\nabla m_i = \frac{\partial m(q)}{\partial q_i}$$

$$= \frac{m(q + de_i) - m(q)}{d}$$
(9)

The six the interpretation of vector  $\nabla m_i$  and  $d$  is

where  $\nabla m_i$  is the *i*-th element of vector  $\nabla m$ , and *d* is a small positive constant.  $e_i$  is the unit vector in the direction of the *i*-th joint.

# 4 MANIPULABILITY OPTIMIZATION FOR LIQUID TRANSFERRING TASK

This section proposes a method to optimize manipulability during liquid transfer by formulating motion planning as an optimization problem, incorporating the minimum jerk trajectory as a constraint.

### 4.1 Minimum Jerk Trajectory Constraint

To suppress sloshing during liquid transfer, it is essential to generate smooth accelerations that do not excite liquid oscillations. For this purpose, the minimum jerk trajectory model is adopted as a constraint in the manipulability optimization problem. The minimum jerk model provides an analytic trajectory with minimized jerk, defined by the third derivative of position, and can be expressed in polynomial form using the start and end conditions of the motion.

The general expression of a minimum jerk trajectory between initial state  $(x_0, v_0, a_0)$  and final state  $(x_f, v_f, a_f)$  is given by

$$x(t) = f(x_0, x_f, v_0, v_f, a_0, a_f, t, t_f)$$
 (10)

where  $t_f$  is the final time. This trajectory guarantees smooth position, velocity, and acceleration profiles. In practical liquid transfer tasks, the final velocity and acceleration are often set to zero ( $v_f = 0$ ,  $a_f = 0$ ), which simplifies the formulation.

For real-time implementation, it is convenient to express the trajectory in recursive form. The position at the next step is computed from the current state (x(t), v(t), a(t)) and the target endpoint  $x_f$  as

$$x(t + \Delta t) = f(x_f, x(t), v(t), a(t), T')$$
 (11)

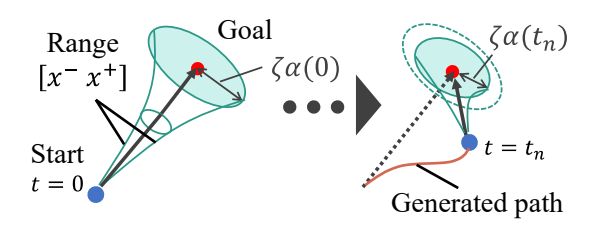
where  $\Delta t$  is the control interval and  $T' = \Delta t/t_f - t$  represents the normalized time increment. This recursive formulation allows the trajectory to be updated at each control step, making it suitable for online optimization.

In the proposed framework, the minimum jerk trajectory is not treated as an additional objective, but rather as an inequality constraint on feasible motions:

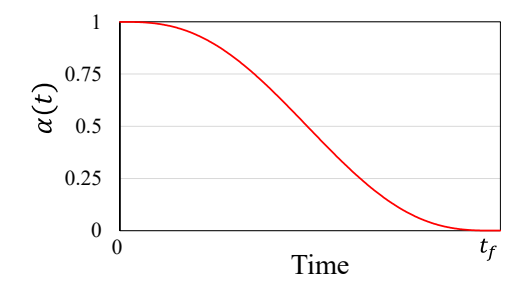
$$\dot{x}^- \le \dot{x} \le \dot{x}^+ \tag{12}$$

where the bounds  $\dot{x}^-$ ,  $\dot{x}^+$  are derived from the minimum jerk trajectory. To account for the trade-off between manipulability and trajectory tracking, a deviation parameter  $\zeta$  and a scaling function  $\alpha(t)$  are introduced:

$$v^{\pm} = \dot{f}\left(x_f \pm \zeta \alpha, x(t), v(t), a(t), T'\right) \tag{13}$$



(a) Feasible search region defined by deviation parameter  $\zeta$  and scaling coefficient  $\alpha(t)$ .



(b) Time profile of scaling coefficient  $\alpha(t)$ .

Figure 2: Concept of minimum jerk trajectory constraint.

Here,  $\zeta \ge 0$  represents the maximum allowable deviation from the nominal trajectory, while  $\alpha(t)$  is a time-varying coefficient that gradually decreases from 1 at the start of the motion to 0 at the end. This flexible constraint design enlarges the search space at the beginning of the motion and tightens it near the goal, thereby reducing computational load while ensuring convergence to the target. In this formulation, v represents the linear velocity subject to inequality constraints, while the angular velocity  $\omega$ is determined to satisfy the tilting condition in (1) at every step. Thus, the container orientation is continuously adjusted to align with the resultant acceleration vector, ensuring sloshing suppression during the transfer. Moreover, any sudden change in deviation must be gradual, as it may lead to abrupt shifts in the search range. Based on these conditions,  $\alpha$  was also derived using the minimum jerk model, along with the trajectory. Figure 2 illustrates this concept: (a) the feasible region defined by the flexible constraint shrinks as the task approaches completion; (b) the scaling coefficient  $\alpha(t)$  decreases smoothly from 1 to 0 according to the minimum jerk model.

Combining these elements, the constraints of the optimization problem for liquid transfer can be expressed as:

$$\dot{x} = J(q)\dot{q}$$

$$q^{-} \le q \le q^{+}$$

$$\dot{q}^{-} \le \dot{q} \le \dot{q}^{+}$$

$$\dot{x}^{-} \le \dot{x} \le \dot{x}^{+}$$

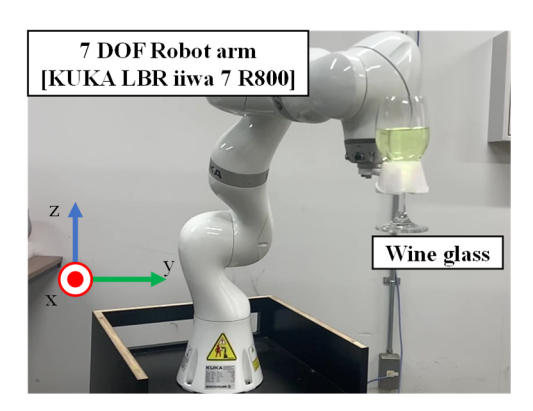


Figure 3: Experimental setup.

with

$$\dot{x}^{\pm} = \begin{bmatrix} v^{\pm} \\ \omega^{\pm} \end{bmatrix}$$
 
$$v^{\pm} = \dot{f}(x_f \pm \zeta \alpha, x(t), v(t), a(t), T')$$

By embedding the minimum jerk model as a constraint rather than as part of the cost function, the optimization remains computationally lightweight. This design is essential for real-time liquid transfer, where both manipulability enhancement and sloshing suppression must be achieved simultaneously.

### 4.2 Experimental Results

To validate the proposed method, liquid transfer experiments use a KUKA LBR iiwa 7 R800 (7 DOF). The setup is shown in Figure 3. A wine glass was transported from the origin (0, 0, 0) to a position 0.5 m along the y-axis within 2.0 s. Trajectory and manipulability were evaluated for various values of  $\zeta$ , representing the maximum deviation. The case with  $\zeta = 0$ , where manipulability is not considered, is defined as the reference trajectory.

In this study, proposed method is evaluated under two conditions: Scenario A, a reference trajectory with high manipulability, and Scenario B, a reference trajectory with low manipulability that passes near a singularity.

### 4.2.1 Scenario A: High Manipulability Trajectory

Figure 4 shows the transport trajectories, while Figure 5 presents the corresponding manipulability, normalized by the robot's maximum value. As  $\zeta$  increases, trajectory deviation becomes more pronounced. At  $\zeta = 0$ , the trajectory is a straight line, reflecting the minimum jerk model without manipulability optimization.

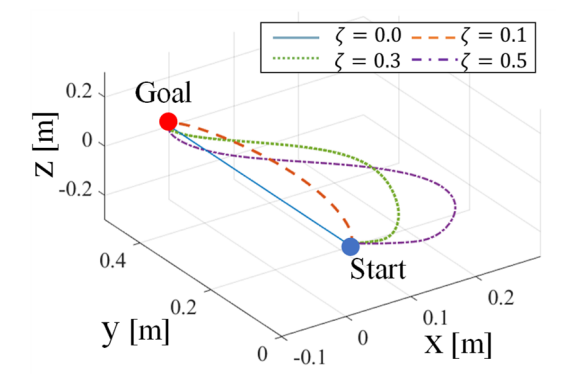


Figure 4: Liquid transferring trajectory (Scenario A).

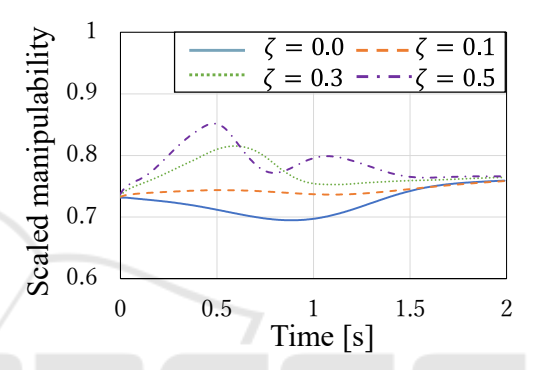


Figure 5: Scaled manipulability (Scenario A).

Figure 5 indicates that the proposed method maintains high manipulability across all conditions. The reference trajectory ( $\zeta=0$ ) results in lower manipulability, suggesting limited kinematic performance and potential instability near singularities. In contrast, optimized trajectories avoid such regions, confirming the method's effectiveness. Notably,  $\zeta=0.3$  achieves a favorable balance between trajectory deviation and manipulability.

The observed increase in manipulability with larger  $\zeta$  suggests that the most favorable postures lie away from the reference path. Minor differences in final manipulability are attributed to jerk minimization delays. Since  $\zeta=0.5$  shows the largest arrival error, adjusting the constraint coefficient  $\alpha$  in real time is recommended.

## **4.2.2** Scenario B: Low Manipulability Trajectory

Figure 6 shows the transport trajectories, while Figure 7 presents the corresponding manipulability. Similar to Scenario A, trajectory deviation increases with larger  $\zeta$  values, and manipulability generally improves as  $\zeta$  increases. The reference trajectory

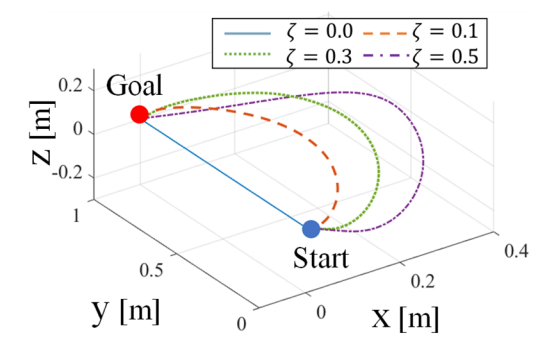


Figure 6: Liquid transferring trajectory (Scenario B).

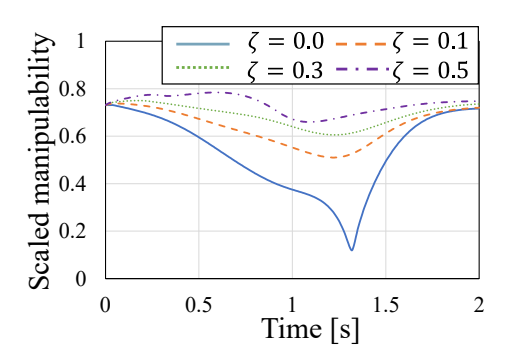


Figure 7: Scaled manipulability (Scenario B).



Figure 8: Liquid transfer using tilting motion control. The red lines show the glass's central axis and liquid surface's orientation. The different lengths of the vertical axis represent the tilt in the depth direction (t = 0.5 s, 1.5 s).

exhibits manipulability values near zero, whereas the proposed method effectively maintains higher manipulability, even for  $\zeta = 0.1$ , enabling singularity avoidance.

These results indicate that manipulability decreases near singularities, and the proposed method effectively avoids such configurations. By formulating sloshing suppression as a manipulability optimization problem, the method simultaneously enhances both manipulability and vibration suppression. Under Scenario B, the method demonstrates effectiveness for singularity avoidance.

Finally, Figure 8 illustrates the motion generated by the proposed method. The container tilt aligns with the direction normal to the liquid surface, confirming the effectiveness of the control. The average and maximum computation times are summarized in Table 1. By avoiding a complex objective, the proposed method achieved computation times below 10 ms in all cases, sufficient for 100 Hz real-time control. A wider flexible constraint slightly increased computation time, reflecting the expansion of the feasible search space.

Table 1: Computation time under different constraints.

Condition ζ	0.0	0.1	0.3	0.5
Avg. time [ms]	0.182	0.472	0.807	1.08
Max. time [ms]	0.612	1.02	1.69	3.06

### 5 CONCLUSIONS

This study proposed a manipulability optimization method that accounts for task-specific constraints, such as end-effector speed and orientation during liquid transfer. Trajectories were generated using a minimum jerk model to achieve both vibration suppression and high manipulability. By incorporating trajectory flexibility as a constraint and gradually tightening it, the method ensured timely and feasible motion execution.

Experimental results confirmed that highmanipulability trajectories can be achieved without extending execution time, demonstrating the method's feasibility under time constraints. Although the end time was fixed, further improvements could be made by adapting it to the manipulator's condition. Future work will extend the constraint formulation to both state and joint spaces and explore redundancy resolution in highly constrained tasks.

### REFERENCES

Diavareshkian, M. H., & Khalili, M. (2006). Simulation of sloshing with the volume of fluid method. *Fluid Dynamics & Materials Processing*, 2(4), 299–308.

Dufour, K., & Suleiman, W. (2020). On maximizing manipulability index while solving a kinematics task. *Journal of Intelligent Robotic Systems*, 100(1), 3–13.

- Flash, T., & Hogan, N. (1985). The coordination of arm movements: An experimentally confirmed mathematical model. The Journal of Neuroscience, 5(7), 1688–1703.
- Haowen, Y., Laha, R., Figueredo, L., & Haddadin, S. (2024). Enhanced Dexterity Maps (EDM): A new map for manipulator capability analysis. *IEEE Robotics and Automation Letters*, 9(2), 1628-1635.
- Jin, L., Li, S., La, H. M., & Luo, X. (2017). Manipulability optimization of redundant manipulators using dynamic neural networks. *IEEE Transactions on Industrial Electronics*, 64(6), 4710–4720.
- Kavraki, L. E., Svestka, P., Latombe, J. C., & Overmars, M. H. (1996). Probabilistic Roadmaps for Path Planning in High-Dimensional Configuration Spaces, *IEEE Trans.* on Robotics and Automation, 12(4), 556-580.
- Kennel-Maushart, F., Poranne, R., & Coros, S. (2021).
  Manipulability optimization for multi-arm teleoperation. In *Proceedings of the 2021 IEEE International Conf. on Robotics and Automation (ICRA) (pp. 3956–3962). IEEE.*
- LaValle, S. M., Kuffner, J. J. (2001). Rapidly-exploring random trees: Progress and prospects, Algorithmic and Computational Robotics, 303-307.
- Maric, F., Limoyo, O., Petrovic, L., Ablett, T., Petrovic, I., & Kelly, J. (2019). Fast manipulability maximization using continuous-time trajectory optimization. In Proceedings of the 2019 IEEE/RSJ International Conference on Intelligent Robots and Systems (IROS) (pp. 8258–8264). IEEE.
- Moriello, L., Biagiotti, L., Melchiorri, C., & Paoli, A. (2018). Manipulating liquids with robots: A sloshingfree solution. *Control Engineering Practice*, 78, 129– 141.
- Muchacho, R. I. C., Laha, R., Figueredo, L. F. C., & Haddadin, S. (2022). A solution to slosh-free robot trajectory optimization. In Proceedings of the 2022 IEEE/RSJ International Conference on Intelligent Robots and Systems (IROS) (pp. 223–230). IEEE.
- Muller, M., Charypar, D., & Gross, M. (2003). Particle-based fluid simulation for interactive applications. *In Proceedings of the 2003 ACM SIGGRAPH /Eurographics Symposium on Computer Animation (pp. 154–159). ACM.*
- Wang, X., Li, X., Guan, Y., Song, J., & Wang, R. (2019).
  Bidirectional potential guided RRT\* for motion planning. *IEEE Access*, 7, 95046–95057.
- Yano, K., Higashikawa, S., & Terashima, K. (2001). Liquid container transfer control on 3D transfer path by hybrid shaped approach. *In Proceedings of the 2001 IEEE International Conference on Control Applications (pp. 1168–1173). IEEE.*
- Yano, K., & Terashima, K. (2001). Robust liquid container transfer control for complete sloshing suppression. *IEEE Transactions on Control Systems Technology*, 9(3), 483–493.

- Yoshikawa, T. (1985). Manipulability of robotic mechanisms. *The International Journal of Robotics Research*, 4(2), 3–9.
- Zhang, H., Sheng, Q., Hu, J., Sheng, X., Xiong, Z., & Zhu, X. (2022). Cooperative transportation with mobile manipulator: A capability map-based framework for physical human-robot collaboration. *IEEE/ASME Transactions on Mechatronics*, 27(6), 4396–4405.

### **APPENDIX**

Only the main symbols frequently used throughout the paper are listed here. Other symbols are defined locally in the text.

Table A1: List of symbols.

Symbol	Definition	
q	Joint angle vector	
ġ	Joint velocity vector	
x	End-effector pose (position and orientation)	
$\dot{x} = [v^T  \omega^T]^T$	End-effector velocity (linear $v$ , angular $\omega$ )	
J(q)	Jacobian matrix of the manipulator	
m(q)	Manipulability index	
ζ	Deviation parameter for flexible constraint	
a(t)	Time-varying scaling coefficient	
$\theta$	Container tilt angle [rad]	
$t, t_f$	Time, final time	